Bond analysis model of deformed bars to concrete

O.C. Choi & S.Y. Yang
Soongsil University, Seoul, Korea

ABSTRACT: Bond slip responses between concrete and reinforcement are known to be highly non-linear due to the interfacial properties of the two different materials, steel and concrete. A simple expression is derived to predict bond strength of reinforcing bars with rib deformation to the surrounding concrete for the case of splitting bond failure. Finite element analysis is used to model the confining behavior of concrete cover that provides confinement. The roles of the interfacial properties on bond strength are examined. Values of bond strength obtained using the analytical model are in good agreement with bond test results from previous studies. The analytical model provides insight into interfacial bond mechanisms and the effects of the key variables on the bond strength of deformed bars to concrete.

1 INTRODUCTION

Several researchers have studied the deformation characteristics of ribbed bars to predict the ultimate strength of lapped reinforcing steel using analytical expressions. Notable works among these studies are those by Tepfers (1979), Cairns (1979). Earlier studies have demonstrated that there is a limit to the role of the face angle of ribs, measured with respect to the bar axis, on the bond strength. Lutz & Gergely (1967) showed that slip of a deformed bar with a high (more normal to bar axis-see Fig. 1) face angle causes crushing of the concrete in front of the ribs, producing a flatter (smaller rib face angle) rib. They concluded that high rib face angles are flattened by crushed concrete, which reduces the effective face angle to a smaller value (Fig. 1).
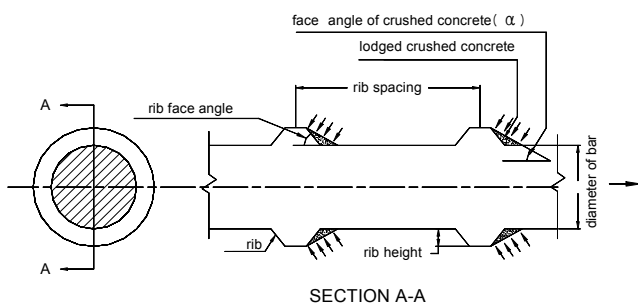

Figure 1. Flattened rib face angle by concrete crouching (Tepfers 1979).

The importance of the interfacial properties between steel bars and concrete, as well as bar geometries has been addressed in studies of epoxy-coated bars. Work by Choi et al. (1991) has demonstrated that the lower relative bond strength of coated bars is due to the lower coefficient of friction and cohesion between concrete and epoxy-coated surfaces than that obtained for uncoated surfaces. They have also demonstrated that the relative bond strength of epoxy-coated bars compared to uncoated bars can be increased by increasing the relative rib area of bars.

2 BOND RESISTANCES IN SPLITTING AND SHEARING RAILURE

A splitting failure occurs in the concrete along the bar when cover or bar spacing is insufficient to resist the lateral concrete tension resulting from the wedging action of the bar deformations. As in a previous study by Cairns (1979), this wedging action makes it possible to resolve bond forces into normal stress σ_n and tangential shear stress τ as shown in Figure 2. The resultant of normal components along the bar is what places the surrounding concrete in tension.
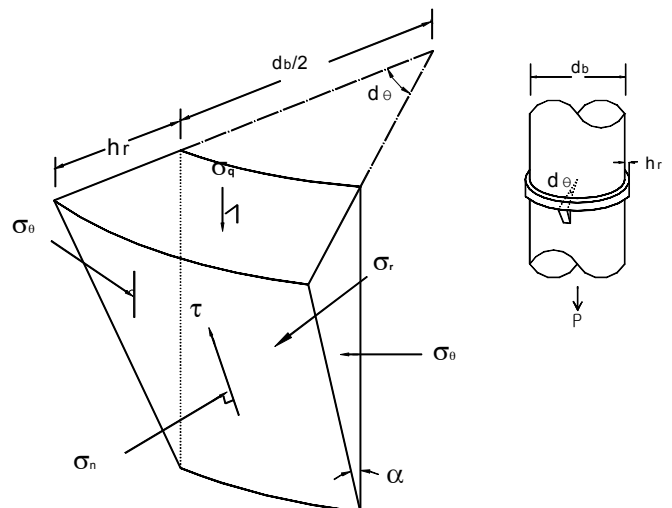

Figure 2. Stresses acting on rib of bar (Cairns 1979).

Concrete under the bearing side of a rib is known to be in a state of tri-axial compression with a major principal stress, the bearing stress, σ_q, on the rib acting parallel to the bar axis. Normal to the bearing stress, the minor principal stress σ_r acting radial occurs around the bar. As the radial force, the wedging force is applied to the concrete cover and confining bars. Splitting occurs when the wedging force exceeds the ultimate confinement strength of the concrete cover.

Bond force equal to the sum of the bearing stress on the rib area along the bonded length, T_1, is given by

$$T_1 = A_r \frac{l_b}{s_r} \sigma_q \qquad (1)$$

in which A_r = projected area of rib parallel to the bar axis, approximated by $A_r = \pi d_b h_r$ where h_r is the rib height, l_b/s_r = number of ribs along the bonded length, l_b, σ_q = bearing stress on the bar rib acting parallel to the bar axis.

The frictional force between the concrete and the steel (Fig. 3) on the inclined surface of the rib may be represented using the Mohr-Coulomb relation,

$$\tau = c + \mu\,\sigma_n \qquad (2)$$

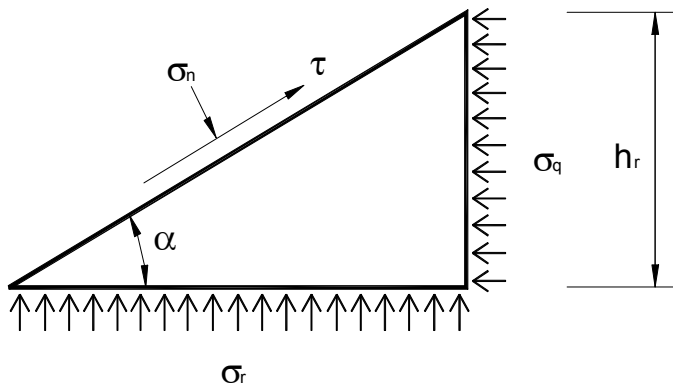where c = cohesion, μ = coefficient of friction, σ_n= normal stress.

Figure 3. Stresses along interface with angle of α.

Suppose the stresses along the interface with an angle of α are in equilibrium with the sliding force by σ_q and the normal force by σ_r. σ_q in Figure 3 is given by

$$\sigma_q = \sigma_r \frac{(1+\mu\cot\alpha)}{(1-\mu\tan\alpha)} + \frac{c}{\sin\alpha(\cos\alpha - \mu\sin\alpha)} \qquad (3)$$

Equation (3) is substituted into Equation (1) to obtain

$$T_1 = A_r \frac{l_b}{s_r}\left(\sigma_r \frac{(1+\mu\cot\alpha)}{(1-\mu\tan\alpha)} + \frac{c}{\sin\alpha(\cos\alpha - \mu\sin\alpha)} \right) \qquad (4)$$

where σ_r acting radially around the bar axis applies to concrete cover as radial stress. The radial stress σ_r acts over a distance of $h_r \cot\alpha$ below the rib, and exerts a bursting force on the concrete around the bar. Figure 4 shows the force exerted by σ_r under one rib over a short length of the bar circumference (Cairns 1979). The component of force in the x-direction is

$$df_x = \sigma_r h_r \cot\alpha \frac{d_b}{2} d\theta \cos\theta \qquad (5)$$

The summation of the component force on the perimeter is given by

$$f_x = \int_{-\frac{\pi}{2}}^{\frac{\pi}{2}} (\sigma_r h_r \cot\alpha) \frac{d_b}{2} d\theta \cos\theta = \sigma_r \cot\alpha h_r d_b \qquad (6)$$

Total bursting force of σ_r on the bonded length in the x-direction is given by

$$F_x = \frac{l_b}{s_r} f_x = \left(\frac{l_b}{s_r}\right)(\sigma_r \cot\alpha h_r) d_b \qquad (7)$$

Equation (7) is substituted into Equation (4) to obtain

$$T_1 = A_r \frac{l_b}{s_r}\left(\frac{F_x}{\frac{l_b}{s_r}\cot\alpha h_r d_b} \frac{(1+\mu\cot\alpha)}{(1-\mu\tan\alpha)} + \frac{c}{\sin\alpha(\cos\alpha - \mu\sin\alpha)} \right) \qquad (8)$$

In addition, the cohesion of bar surface on the bonded length may be expressed as

$$T_2 = \pi d_b l_b c \qquad (9)$$

Thus, the total bond force T is given by

$$T = T_1 + T_2 \qquad (10)$$

Combining Equations (8), (9) and (10) results in the final equation to predict bond strength, which is expressed as follows.

$$T = F_x \pi \tan\alpha \frac{(1+\mu\cot\alpha)}{(1-\mu\tan\alpha)} + A_r \frac{l_b}{s_r} \frac{c}{\sin\alpha(\cos\alpha - \mu\sin\alpha)} + \pi d_b l_b c \qquad (11)$$

The second and third terms of the right side of Equation (11) are due to cohesion between the reinforcing bar and the concrete that is supposed to diminish, thus increasing slip of reinforcing bars.
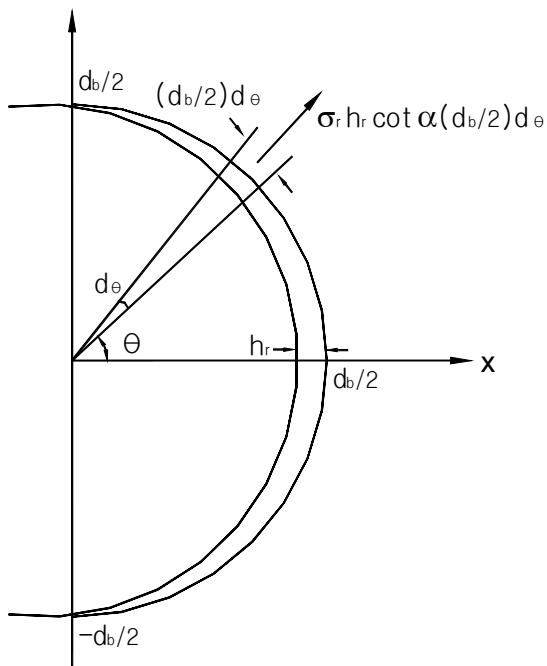
Figure 4. Radial stress around bar circumference (Cairns, 1979).

3 FINITE ELEMENT ALNALYSIS

3.1 *Model for concrete confining force*

F_x in Equation (11) is the confining force. It is made up of the resistance by concrete cover or by transverse reinforcement, including stirrups or ties. Resistance by cover is related to the splitting tensile strength of concrete, the magnitude of the fracture energy, and the area of failure surface.

The confining force by cover, F_x, is obtained from the finite element study to simulate surface fracture of concrete cover. The cracks observed in the bond test specimens, mainly beam-end specimens, consistently reveal a splitting failure with a dominant fracture surface or running crack. Hillerborg et al. (1976) proposed the fictitious crack model for predicting crack propagation in concrete. In a concrete specimen, it is presumed that, although the tensile strength is reached, a micro-cracked zone, the so-called fictitious crack, can transfer tensile stress. This stress transfer capability is represented as a stress-displacement curve (Petersson 1980). As the crack width reaches w_0, all of the energy that can be absorbed by the concrete is accounted for and the tensile stress becomes zero. The area under this stress-displacement curve represents the energy absorbed per unit area of the crack surface in opening the crack from zero to w_0 and can be calculated as:

$$G_c = \int_0^{w_o} \sigma dw \qquad (12)$$

in which, G_c is the fracture energy, σ is the tensile stress at the crack, w is the crack width, and w_0

is the displacement at which the tensile stress in the concrete becomes zero.

For the current study, the fictitious crack model is employed in the finite element analysis to represent the splitting crack that forms at the specimen centerline. The crack is represented using rod elements perpendicular to a defined fracture plane located at the specimen centerline. In the initial elastic response prior to the rod elements attaining a tensile stress sufficient to begin cracking, the elements are intentionally modeled as very stiff, using a modulus of elasticity of 2.75 GPa. For the current study, regarding the area inside this stress-displacement curve, the fracture energy is assumed to be 100 kN/m, a G_c value corresponding to the compressive strength of the concrete used in this study. The tensile strength is set at 2.75 MPa based on a 41.5 MPa compressive strength. This stress-displacement relationship is converted to a stress-strain function for the nonlinear material model of the rod elements, as shown in Figure 5.
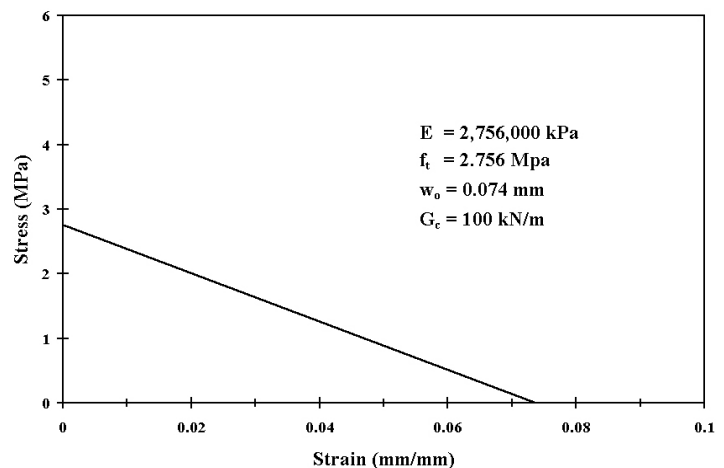

Figure 5. Stress-strain function for rod elements.

3.2 *Analysis and numerical results*

Analysis is carried out in two steps. The first step represents the splitting of the concrete, while the next step represents the interfacial action using Equation 11. In the first step, previous finite element analysis results for the beam-end specimen are used to obtain the confining force, F_x. The element model for the beam-end specimen included representations for the deformed bar, the concrete, and the splitting crack plane, connected by the rod element. To obtain the lateral load-lateral displacement curves, loads were applied at the nodes where the reinforcing bar would be located. In the second step, test results for beam-end specimens with 1, 2 and 3 d_b covers are used to determine the interfacial properties such as c, μ, α. From the comparison between test and analysis results, the cohesion and coefficient of friction are finally taken as 1.5 MPa and 0.45. The effective rib face angle is taken as 30 de-

grees, although the value appears to change depending on the magnitude of concrete cover. The procedures to determine these values are described and discussed in detail as follows.

4 DISCUSSIONS

4.1 *Comparison with test results*

The performance of the analytical model is examined on the basis of load slip response. Non-linearity for the curves from the model is mainly due to the inelastic properties of cover concrete, specifically the lateral load–displacement curves. At the peak load and beyond, the models exhibit a typical bond failure as shown in Figure 6. The model with 1 d_b cover possesses a relatively flat load-slip curve. Bond strengths from this analysis are 173.2, 219.6 and 271.0 kN for the models with 1, 2 and 3 d_b covers, respectively, compared to average bond strengths of 142.7, 217.4 and 271.8 kN for the beam-end specimens from the experimental results as in Table 1 and Figure 8. A further comparison can be made using the empirical equations developed by Orangun et al. (1977), Darwin et al. (1996). From the design equation proposed by Orangun et al.(1977), neglecting the effect of transverse reinforcement, the force in a bar at splice failure, T_b, can be expressed as,

$$T_b = \left(1.2 + \frac{3C}{d_b} + \frac{50d_b}{l_d}\right) \times \sqrt{f_c'} \times \pi d_b l_d \qquad (13)$$

where C is concrete cover, in inches. From the proposed equation by Darwin et al.(1996),

$$T_b = \left[63l_d(C_m + 0.5d_b) + 2130A_b\right]\left(0.1\frac{C_M}{C_m} + 0.9\right) \times f_c'^{1/4} \quad (14)$$

Table 1. Comparison of bond strength: analyses, test results and empirical equations.

Comparison	d_b (mm)	Cover (mm)	Bond strength (kN)		C/d_b	Strength ratio normalized 2 d_b cover
Test results by Choi et al. (1990)*	25	25	143.1 144.6 140.4	142.7	1.0	0.66
		50	231.3 212.0 208.8	217.4	2.0	1.00
		75	293.8 249.8	271.8	3.0	1.25
Eq.(13)[†]	25	25	91.4		1.0	0.77
		50	117.9		2.0	1.00
		75	144.0		3.0	1.22
Eq. (14)[†]	25	25	120.6		1.0	0.94
		50	128.3		2.0	1.00
		75	140.9		3.0	1.10
Eq. (11)*	25	25	173.2		1.0	0.79
		50	219.6		2.0	1.00
		75	271.0		3.0	1.23

* From beam-end specimens
[†] From splice tests

where C_M and C_m are the maximum and minimum values of clear spacing, side cover and bottom cover, in inches. For each equation, the ratios of the bond strengths obtained at 1, 2 and 3 d_b covers to the value at 2 d_b cover are compared to the analytical results in this study and the previous test results as in Figure 7. The analytical solution closely matches both the curve generated by Equation 13 (Orangun et al. 1977) and the test data.
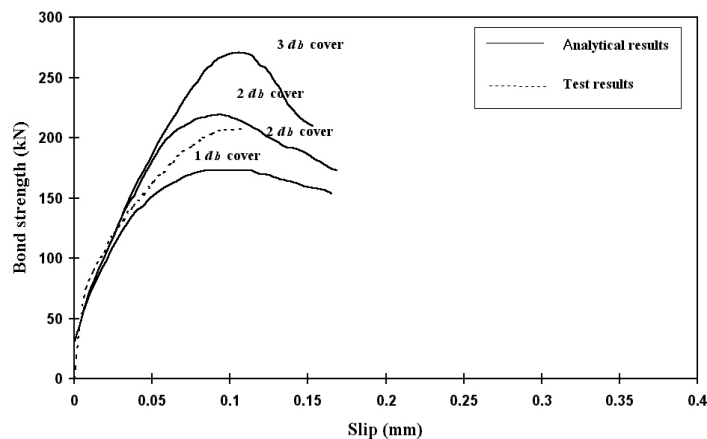

Figure 6. Bond force-slip curves for models with 1, 2, and 3 bar diameter covers.
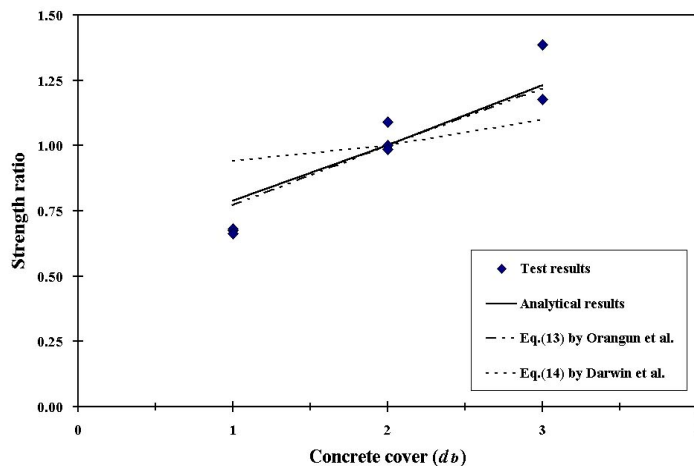

Figure 7. Strength ratio normalized to 2 bar diameter cover versus cover: analytical results, tests results and empirical equations.

4.2 *Fracture properties of concrete cover*

Fracture properties of concrete cover can be examined by comparing the test data to the results from the analysis. Since the predicted bond strengths for three different covers match the test results and the empirical equations, the effect of the splitting cracking appears to be well represented by concrete fracture theory. From Equation (11), it is observed that concrete cover provides a confining force that is directly proportional to bond strength after cohesion is lost. The constants of the proportion mainly consist of the coefficient of friction and the effective of rib face angle.

4.3 *Effective rib face angle and deformation patterns*

The crushing of concrete was reported to produce the effective rib face angle of 30 to 40 degrees by Lutz and Gergely in their early study. The effective rib face angle not only depends on material properties but also structural properties. Assuming the upper limit for the coefficient of friction as 0.56, the effective face angle could be approximately within the range between 22 and 27 degrees for 2 d_b cover according to the results plotted in Figure 8. With the coefficient of friction as 0.45 taken in this study, the effective rib face angle is approximately within the range between 26 and 33 degrees. It is safer to propose the range of the angle as between 25 and 35 degrees, that are smaller than the real rib face angle. The proposed ranges for the effective rib face angle and the coefficient of friction are shown in Figure 8. The first term of the right part in Equation (11) shows that the mechanical friction component is independent of the relative rib area after the loss of cohesion.
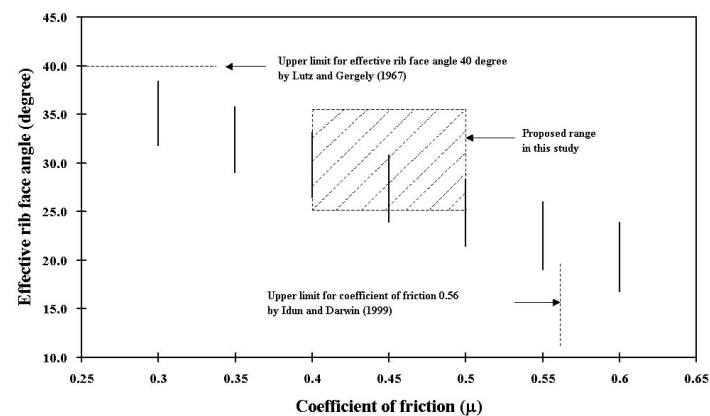

Figure 8. Coefficient of friction versus average range of effective rib face angle for 1, 2, and 3 bar diameter cover.

5 CONCLUSIONS

A simple expression to predict bond strength is derived to analyze interfacial geometry between ribbed bars and concrete. The predicted bond strengths agree well with the test results and empirical equations. Splitting cracks in cover is well represented using a fracture theory. The bond-slip response could become brittle and closer to that of the test specimen, if non-linear approximation of fracture energy for the cover concrete were used. The effective rib face angle ranges between 25 and 35 degrees, which is lower than the actual rib face angles. The relative rib area has little effect on the bond strength of deformed bars when the bars are not confined by transverse reinforcement and failure is only governed by the splitting mode.

REFERENCES

Cairns, J., 1979. "An Analysis of the Ultimate Strength of Lapped Joints of Compression Reinforcement," *Magazine of Concrete Research*, V. 31, No. 106, Mar., pp. 19-27.

Choi, O. C., Hadje-Ghaffari, H., Darwin, D. and McCabe, S. L., "Bond of Epoxy-Coated Reinforcement to Concrete: Bar Parameters," *ACI Materials Journal*, V.88, No. 2, 1991, Mar-Apr., pp. 207-217.

Choi, O. C. and Lee, W. S., 2002, "Interfacial Bond Analysis of Deformed Bars to Concrete," *ACI Structural Journal*, V. 99, No. 6, Nov.-Dec., pp. 750-756.

Hillerborg, A., Modeer, M., and Petersson, P. E., 1976, "Analysis of Crack Formation and Crack Growth in Concrete by Means of Fracture Mechanics and Finite Elements," *Cement and Concrete Research*, V. 6, No. 6, Nov., pp. 773-782.

Idun, E. K. and Darwin D., 1999, "Bond of Epoxy –Coated Reinforcement: Coefficient of Friction and Rib Face Angle," *ACI Structural Journal*, V.96, No. 4 July-Aug., pp. 609-615.

Orangun, C. O., Jirsa, J. O., and Breen, J. E., 1977, "A Reevaluation of Test Data on Development Length and Splices,' *Journal of the American Concrete Institute*, V. 74, No. 3, Mar., pp.114-122.

Petersson, P-E., 1980, "Fracture Energy of Concrete: Method of Determination," *Cement and Concrete Research,* V.10, No. 1, Jan., pp. 79-89.

Tefers, R.,1979 "Cracking of Concrete Cover Along Anchored Deformed Reinforcing Bars," *Magazine of Concrete Research*, V. 31, No. 106, Mar., pp. 3-12